Clays and Clay Minerals, Vol. 66, No. 6, 500–514, 2018.

REMOVAL OF PHOSPHATE BY IVORY COAST SHALE IN A HOMOGENEOUS REACTOR AND UNDER HYDRODYNAMIC CONDITIONS: INFLUENCE OF SOLUBLE SPECIES

D. E. Kpannieu[1,2], C. Ruby[1], L. Coulibaly[2], M. Abdelmoula[1], and M. Mallet[1]

[1]Laboratoire de Chimie Physique et Microbiologie pour l'Environnement - LCPME UMR 7564 CNRS-Université de Lorraine, 405 rue de Vandoeuvre, 54600 Villers-lès-Nancy (France)

[2]Laboratoire d'Environnement et Biologie Aquatique, Université Nangui Abrogoua, 02 BP 801, Abidjan 02 (Côte d'Ivoire)

Abstract—Developing low cost and effective phosphate adsorbents is crucial to prevent eutrophication of natural waters. Here, phosphate removal by a natural and abundant shale from the Ivory Coast was investigated in both batch and column experiments with special attention devoted to understand the adsorption process. Batch experiments were carried out to assess the influence of initial phosphate concentration, sorbent dosage, contact time, and pH on phosphate removal. The phosphate removal efficiency increased with increased shale dosage while phosphate uptake decreased. Aqueous Ca, Mg, Al, and Fe species concentrations decreased in the presence of phosphate. Additionally, phosphate uptake strongly decreased with pH increases in the range 2−11, but then increased at pH 12. The kinetics were well described using a pseudo-second order model, and Langmuir adsorption isotherms were used for the equilibrium surface reactions. Adsorption to nanoparticles of goethite was hypothesized to be the major phosphate removal mechanism in the pH range 4−10. Column experiments with a flow rate of 1 mL min^{-1} and an initial phosphate concentration of 25 mg L^{-1} showed a breakthrough point at a V/Vp value of ~17, where V is the volume of phosphate solution added to the column and Vp is the pore volume. A V/Vp value of ~17 corresponded to a phosphate uptake of 0.17 mg/g, which was in agreement with the batch experiments. Column experiments revealed a strong correlation between the aqueous concentrations of Ca, Mg, Al, and Fe species and phosphate removal and, thus, suggest that phosphate removal by the shale occurred by aqueous dissolution/precipitation.

Key Words—Eutrophication, Phosphate Uptake, Shale, Sorption Mechanism.

INTRODUCTION

Phosphate is well known to be an essential nutrient for the growth of plants and biological organisms, but an excessive supply of phosphates causes eutrophication of the receiving waters. Dramatic growth of algae, fish kills, and degraded water quality are some of the critical side effects of eutrophication. Excess phosphate in aquatic environments originates from anthropogenic activities, such as industrial, agricultural, and household uses, such as phosphate detergents. Additionally, the lack of wastewater treatment has become a major environmental concern, especially in developing countries where conventional techniques, such as biological P treatments and chemical precipitation, cannot be implemented because of the high cost and technological complexity. For example, the Ebrié lagoon is in the Ivory Coast and eutrophic status makes a large area of the lagoon unsafe for habitation sites and for lucrative activities, such as bathing and fishing (Briton *et al.*, 2007; Yao *et al.*, 2009; Koffi *et al.*, 2009; Tuo *et al.*, 2012).

* E-mail address of corresponding author:
martine.mallet@univ-lorraine.fr
DOI: 10.1346/CCMN.2018.064118

Phosphorus has been identified in many studies (Aerts and Chapin, 2000; Nedja and Laskri, 2015) as the limiting factor in the eutrophication of fresh waters (Comeau *et al.*, 1986). The total P content of the effluents and streams that discharge directly into lakes and dams is regulated by national and international water quality standards with maximum concentration limits that range from 0.1 to 2.0 mg L^{-1} P and with the generally accepted limit of 1.0 mg L^{-1} P (Tykesson, 2005).

Among the available chemical methods to decrease phosphate concentrations in water and, thus, limit eutrophication processes, adsorption has been recognized as a low cost, effective, and promising method. The search for materials with high P sorption capacities has attracted growing interest in recent years, although the main challenge has been to find a low cost and easily available material. These phosphate adsorbents include blast furnace slags (Johansson, 1999), apatite (Molle *et al.*, 2005; Molle *et al.*, 2011), shale (Drizo *et al.*, 2000), laterite (Wood and McAtamney, 1996), fly ash (Can and Yildiz, 2006; Chen *et al.*, 2007), bauxsol™ (Akhurst *et al*, 2006), shell sand and Filtratite-P® (Ádám *et al.*, 2007), and electric-arc furnace steel slag and serpentinite (Drizo *et al.*, 2006). Several review articles that concern phosphate removal by various filtration materials were also reported (Johansson, 2006, Vohla *et al.*, 2011, Wendling *et al.*, 2013, Loganathan *et al.*, 2014).

Shale is a natural geological material that is easily available in large amounts in the Ivory Coast where the eutrophication of Ebrié lagoon is dramatic in some areas (*e.g.* excessive growth of algae that induces fish kills), but also releases toxic gases (H_2S) and causes navigation problems for fishermen. Shale is a cost-effective and environmentally friendly material that contains Fe, Ca, and Al and was expected to be a promising material to decrease phosphate concentrations in wastewater before discharge into the Ebrié lagoon (Drizo *et al.*, 1999; Arias and Brix, 2005; Vohla *et al.*, 2011).

Only a few studies devoted to phosphate removal by shale are in the published literature and the studies essentially focused on measuring aqueous phosphate concentrations (Drizo *et al.*, 1999; Kaasik *et al.*, 2008; Cyrus and Reddy, 2010; Jiang *et al.*, 2014). In those previous studies, no specific attempt was made to investigate the removal process by shale. Two possible mechanisms of phosphate removal, however, were mentioned: (i) phosphate adsorption on shale particle surfaces, and (ii) dissolution of Ca and Mg species followed by the precipitation of Ca or Mg phosphate minerals. The goal of the present study was to obtain a deeper understanding of the phosphate removal process by shale both in homogeneous aqueous suspensions and under hydrodynamic conditions. For this purpose, aqueous phosphate and other soluble species, such as Ca, Mg Fe, and Al, were determined both in batch and column experiments. A comparison of the results obtained in these conditions will highlight modification of the shale sorption/dissolution properties during phosphate removal. Another important purpose of the work is to evaluate if Ivory Coast shale can be used as a cost effective and natural solution to reduce P concentrations in wastewaters.

EXPERIMENTAL

Materials

Chemicals. All reagents (*i.e.*, sodium phosphate monobasic dehydrate ($NaH_2PO_4{\cdot}2H_2O$), Sigma Aldrich, $\geqslant$ 99%; sodium hydroxide (NaOH), Carlo Erba, >99%; and hydrochloric acid (HCl), Prolabo, 36%) were of analytical grade. Deionized water was produced using a Millipore Milli-Q water purifier (Mllipore Sigma, Burlington, Massachusetts, USA) and had an electrical resistance of 18.2 MΩ-cm.

Adsorbent. Samples of shale were collected from the Toumodi region (*i.e.* Lomo North site) in the central part of Ivory Coast (Côte d'Ivoire). Large blocks of shale collected from the soil were first crushed manually with a hammer into coarse fragments, washed several times to remove adherent surface particles, and dried at 50ºC for 24 h. The samples were then manually crushed again to produce finer particles and sieved to obtain 1−2 mm particles. Samples were then washed again using deionized water and dried at 70ºC for 24 h before use. Sample powders of $\leqslant$400 μm were obtained by manual grinding of the 1−2 mm samples in an agate mortar. The chemical composition and some physical parameters of the shale were determined (Table 1). The chemical composition of the shale was expressed as a percent of the major oxides (Table 1) SiO_2 (~56.8%), Al_2O_3 (~17.5%), and Fe_2O_3 (~10.2%).

Batch adsorption experiments

All the experiments were conducted in polypropylene vessels. All glassware and plasticware were cleaned in 36% HCl before use and rinsed with deionized water and ethanol. Experiments were performed at room temperature. The pH measurements were carried out using an

Table 1. Chemical composition (wt.%) and some physical parameters of a naturally occurring shale sample from Lomo North (Ivory Coast). The porosity was determined in triplicate using a volumetric method to determine the volume of water (V_w) required to saturate a known volume of shale (V_s). The porosity (ε) was determined using the formula $\varepsilon = V_w/V_s \times 100$. The particle-size distribution was analyzed and determined in triplicate using conventional dry-sieving techniques. Cumulative grain-size distribution plots were used to estimate the maximum size of particles that constitute 10% (*d10*) and 60% (*d60*) of the shale sample. The uniformity of the cumulative particle-size distribution (the uniformity coefficient, *CU*) was calculated as the ratio d_{60}/d_{10}.

Chemical composition (%)										
SiO_2	Al_2O_3	Fe_2O_3	MnO	MgO	CaO	Na_2O	K_2O	TiO_2	P_2O_5	LOI**
56.8	17.5	10.2	0.6	2.1	0.4	0.9	2.4	1	0.1	8.7

Physical characteristics						
Shale (mm)	d_{10} (mm)	d_{60} (μm)	*CU*	Porosity (%)	Bulk density (g cm^{-3})	K* (m s^{-1})
1−2	1.789	0.951	0.53	50	2.4	3.2×10^{-2}

* Saturated hydraulic conductivity; ** Loss on Ignition

https://doi.org/10.1346/CCMN.2018.064118 Published online by Cambridge University Press

Almemo 2690 digital pH meter (Lms Ilmenau, Ilmenau, Germany), and a WTW glass electrode (Xylem Analytics, Weihleim, Germany). Unless otherwise specified, the pH was maintained at a fixed value by the addition of minimum volumes of 0.5 M NaOH or 0.5 M HCl at constant time intervals. Samples were stirred on an orbital shaker at 300 rpm. Batch experiments were carried out using the shale ⩽400 μm fraction.

The effect of sorbent dosage on percent phosphate removal and uptake capacity was examined using a shale sample concentration range of 2−140 g L^{-1} (2, 4, 6, 10, 15, 20, 40, 50, 80, 100, 120, and 140 g L^{-1}) and at various initial phosphate concentrations (5, 25, 75, and 100 mg L^{-1}). Ten mL of solution was withdrawn from the reaction vessels after 24 h and filtered through 0.22 μm polypropylene syringe filters for phosphate analysis by inductively coupled plasma atomic emission spectroscopy (ICP-AES).

The effect of pH on phosphate adsorption was examined using a similar procedure with various initial concentrations of phosphate solutions (5−25 mg L^{-1}) and 80 g L^{-1} of shale, while the pH was maintained at different values in the range 2−12. The samples were sedimented using centrifugation, and the phosphate concentrations in the supernatants were determined after a contact time of 24 h using ICP-AES. All experiments were carried out in duplicate.

Phosphate adsorption kinetics were examined in 1 L Erlenmeyer flasks using initial phosphate concentrations of 5 and 25 mg L^{-1} and a shale powder concentration of 80 g L^{-1} for 96 h. The pHs of the suspensions were maintained at a defined value of 6.5−7.0 by adjustment with 0.5 M NaOH or 0.5 M HCl. Ten mL samples were withdrawn at appropriate time intervals from the reaction vessels and filtered through 0.22 μm polypropylene syringe filters for phosphate and total soluble Ca, Mg, Al, and Fe analyses using ICP-AES.

Adsorption isotherm experiments were carried out at pH 6.5−7.0 in Erlenmeyer flasks that contained 50 mL of various initial phosphate concentrations (5−250 mg L^{-1}) and a constant shale concentration of 80 g L^{-1}. The lowest phosphate concentration of 5 mg L^{-1} was chosen because it is close to the upper concentration limit allowed in the outflow from wastewater treatment plants. The highest concentration of 250 mg L^{-1} was necessary to fully saturate the P adsorption sites on the shale surface. The reaction period was limited to 24 h, which was previously determined from kinetics experiments as sufficient to reach equilibrium. A unique aliquot of 10 mL of solution was, therefore, withdrawn after 24 h for phosphate analysis by ICP-AES.

The Langmuir and Freundlich equations were used to describe phosphate equilibrium adsorption to minerals and were expressed as follows:

$$\frac{C_e}{q_e} = \frac{C_e}{q_m} + \frac{1}{K_L q_m} \quad (1)$$

$$\log q_e = \log K_F + \frac{1}{n} C_e \quad (2)$$

where q_e (mg g^{-1}) is the amount of phosphate adsorbed at equilibrium, K_L is an empirical constant, and q_m (mg g^{-1}) is the theoretical maximum monolayer adsorption uptake in the Langmuir equation; C_e is the equilibrium phosphate concentration in solution (mg L^{-1}) and K_F and n are empirical constants in the Freundlich equation.

The effect of pH on phosphate adsorption was examined using a similar procedure that varied the initial concentrations of phosphate solutions (5−25 mg L^{-1}) with a 80 g L^{-1} shale concentration, while maintaining the pH in the range 2−12. The supernatant phosphate concentrations were determined after a contact time of 24 h. All experiments were carried out in duplicate.

Column experiments

The experiments were carried out in 500 mm long and 37 mm internal diameter Plexiglas™ columns. The columns were packed with 593 g of dried shale (1−2 mm) and were pre-equilibrated with water. The volume of the shale in the columns (V) was 473 mL with a pore volume (V_p) of 236 mL. The flow direction was from the bottom to the top to ensure water-saturated conditions. The upflow mode also allowed the dead volume to be minimized and optimized contact between the solution and the adsorbent. Phosphate solution at a concentration of 25 mg L^{-1} was supplied continuously at either 0.230 ± 0.005 mL min^{-1} (column C1) or 2.30 ± 0.05 mL min^{-1} (column C2) *via* a Watson-Marlow peristaltic pump (Watson-Marlow Ltd, Zollikon, Switzerland). The flow rates were selected to obtain water and shale contact times of 17 h and 1.7 h for columns C1 and C2, respectively. The pH of the solution introduced into the columns was 4.8 and the outflow pH was between 5.6 and 6.6. The phosphate solution was circulated continuously during the first 104 h period and then was stopped during a second 64 h period to study the effect of residence time on phosphate removal. The durations of the 104 h and 64 h column circulation sequences were chosen to simulate a situation that can be encountered in constructed wetlands, where water is often provided discontinuously. The 104 h to 64 h circulation sequence was repeated 9 times for column C1, which corresponded to a total experiment duration of 66 d. The sequence of 104 h (dynamic mode) and 64 h (static mode) was repeated only two times for the experiments performed in column C2. The higher flow rate chosen for the column C2 experiment led to a much earlier phosphate breakthrough. Ten mL samples were collected in the column outflow at appropriate time intervals and filtered through 0.22 μm polypropylene syringe filters before the phosphate and the aqueous Ca,

https://doi.org/10.1346/CCMN.2018.064118 Published online by Cambridge University Press

Mg, Al, and Fe concentrations were analyzed using ICP-AES.

The hydraulic retention time (HRT) was determined using the following equation (Jiang *et al.*, 2014):

$$HRT = \frac{\pi r^2 H \varepsilon}{Q} \quad (3)$$

where, r (cm) is the column radius, H (cm) is the substrate height in the column, ε (%) is the shale porosity, and Q (mL h^{-1}) is the measured flow rate.

The clogging rate (CR) of the column was determined using the following equation:

$$\mathrm{CR}(\%) = \left(\frac{Q_{\mathrm{init}} - Q_{\mathrm{inst}}}{Q_{\mathrm{init}}}\right) \times 100 \quad (4)$$

where Q_{init} (mL min^{-1}) and Q_{inst} (mL min^{-1}) are the initial and instantaneous output flow rates, respectively.

The phosphate uptake of the column q_{col} (mg g^{-1}), which represents the total amount of phosphate adsorbed to the shale, was determined using the following equation (Husein *et al.*, 2017):

$$q_{(\mathrm{col})} = \frac{Q}{m} \times \int_0^t (C_0 - C)dt \quad (5)$$

where Q (L d^{-1}) is the measured flow rate, m (g) is the mass of shale in the column, C_0 (g L^{-1}) is the phosphate concentration in the incoming effluent, and C (g L^{-1}) is the phosphate concentration in the outlet effluent.

Characterization techniques

The mineralogy and chemical properties of Fe in the shale were determined using X-ray diffraction (XRD) and Mössbauer spectrometry. The XRD patterns were obtained using a PANalytical X'Pert Pro Multipurpose diffractometer (PANalytical, Eindhoven, The Netherlands) using Co Kα radiation (λ = 1.78026 Å, 40 kV, 40 mA). Diffraction patterns were collected over a 2θ range of 10–85º using a step size of 0.036º and a nominal time of 3 s per step. Transmission Mössbauer spectrometry (Fast ComTec GmbH, Oberhaching, Germany) was performed using a 50 mCi ^{57}Co source in Rh (Ritverc, St. Petersburg, Russia). The Mössbauer spectra were calibrated relative to the reference spectrum of a 25 μm thick pure Fe foil recorded at room temperature. An Advanced Research Systems cryostat equipped with a closed cycle He station (Advanced Research Systems, Macungie, Pennsylvania, USA) allowed variable temperature measurements between 12 and 300 K.

Residual phosphate (PO_4-P) and total dissolved Ca, Mg, Al, and Fe concentrations were determined using inductively coupled plasma atomic emission spectrometry (ICP-AES) with an Horiba Ultima spectrometer (Horiba, Kyoto, Japan). The removal efficiency R (%) and phosphate uptake q_t (mg g^{-1}) at time t were determined using the following equations:

$$R(\%) = \frac{C_i - C_t}{C_i} \times 100 \quad (6)$$

$$q_t = \frac{(C_i - C_t) \times V}{m} \quad (7)$$

where C_{i} and C_t are the initial and time t phosphate concentrations (mg L^{-1}), respectively, V is the solution volume (in L), and m is the mass of shale (g).

Additionally, phosphate uptake by shale at near equilibrium conditions (q_{e}, mg g^{-1}) was determined using the following equation:

$$q_{\mathrm{e}} = \frac{(C_i - C_{\mathrm{e}}) \times V}{m} \quad (8)$$

where C_{e} is the equilibrium phosphate concentration (mg L^{-1}).

RESULTS AND DISCUSSION

Physicochemical properties of shale

The XRD pattern (Figure 1) indicated that the mineral content of the shale includes quartz (SiO_2), muscovite ($KAl_2(Si,Al)_4O_{10}(OH)_2$), albite ($(Na,Ca)(Si,Al)_4O_8$), and clinochlore ($(Mg,Fe)_5(Si_3Al)O_{10}(OH)_8$). No Fe-based mineral was observed in contrast to the 10.2% Fe_2O_3 value reported in Table 1. Because Fe is well known to play a key role in phosphate adsorption (Alindogan and Tumen, 2001; Mallet *et al.*, 2013), Fe-rich minerals in the shale were more closely examined using Mössbauer spectrometry.

The Mössbauer spectrum was recorded at 12 K (Figure 2) and was fitted with two D_1 and D_2 paramagnetic doublets and two S_1 and S_2 sextets to adjust the magnetic component. The sextet hyperfine parameters, in particular the negative ε = −0.2 mm s^{-1} value of the quadrupole shift of sextet S_1, was identified as goethite (α-FeOOH) and accounted for approximately 1/3 of the total Fe in the sample (Table 2). Goethite required an additional sextet S_2 to take into account the

Table 2. Mössbauer hyperfine parameters for shale calculated from the spectra in Figure 2. CS = the center shift with respect to α-Fe at room temperature; Δ = quadrupole splitting or ε = quadrupole shift; H = hyperfine magnetic field; and RA = the relative area.

Component	CS (mm s^{-1})	Δ or ε (mm s^{-1})	H (kOe)	RA (%)
D_1	0.470	0.836	–	55
D_2	1.272	2.71	–	14
S_1	0.6	−0.2	480	23
S_2	0.56	−0.08	500	8

https://doi.org/10.1346/CCMN.2018.064118 Published online by Cambridge University Press

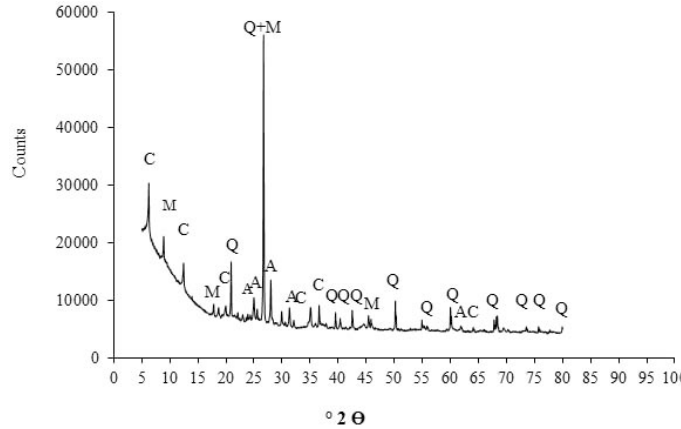

Figure 1. XRD pattern of natural shale sample from Lomo North (Ivory Coast). The following abbreviations were used: Q = quartz; A = albite; M = muscovite, and C = clinochlore.

line broadening. XRD peaks characteristic of goethite were not observed, however, which suggests that it is a poorly crystalline Fe (oxyhydr)oxide (Figure 1). The other Fe atoms (2/3) consisted of ferric species (doublet D_1) and ferrous species (doublet D_2), which were structural substitutions in the various silicate minerals identified using XRD (*i.e.* albite, muscovite, and clinochlore). The majority of the Fe species (86%) were thus present in the ferric state Fe(III).

Phosphate adsorption experiments: batch tests

Effect of initial phosphate concentration and contact time. In a first step, the effects of both initial phosphate concentration and contact time on phosphate removal by shale were examined (Figures 3 and 4). An increased percent phosphate removal with time was observed until a plateau was reached (Figure 3). In addition, the percent phosphate removal at time *t* strongly decreased with increases in initial phosphate concentration. Of particular interest was that the percent phosphate removal was smaller than 100%, which made it possible to determine the maximum phosphate uptake for these two initial phosphate concentrations. Phosphate uptake as a function of time (Figure 4), not surprisingly, displayed the same curve pattern as that observed for phosphate removal (Figure 3) and was in agreement with previous studies (Namasivayam and Prathap, 2005; Wu *et al.*, 2012). The phosphate adsorption was rapid in the initial stages and then gradually decreased with time until equilibrium conditions were reached. Equilibrium was reached in

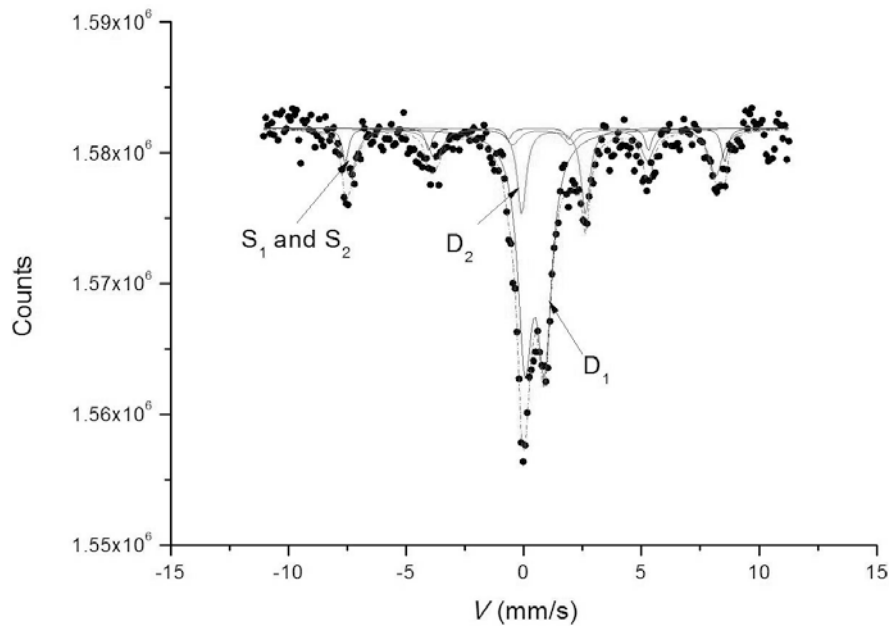

Figure 2. ^{57}Fe Mössbauer spectrum at 12K of a natural shale sample from Lomo North (Ivory Coast).

https://doi.org/10.1346/CCMN.2018.064118 Published online by Cambridge University Press

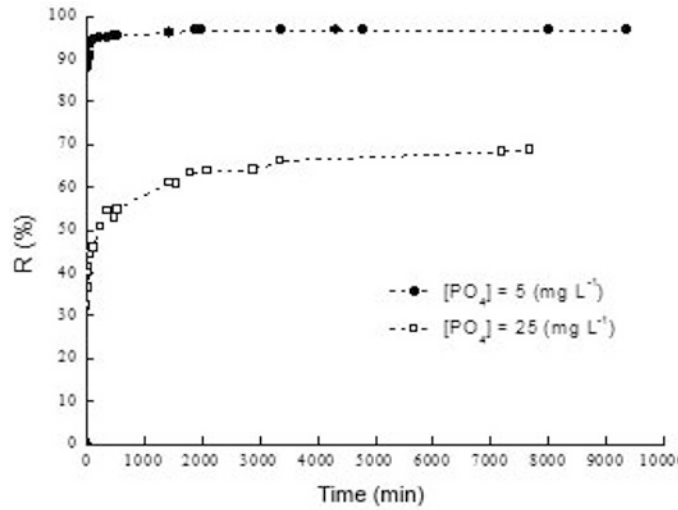

Figure 3. Effect of contact time at two initial phosphate concentrations on phosphate removal for a shale concentration of 80 g L^{-1} at pH ≅ 7.

about 60 min and 3500 min for initial phosphate concentrations of 5 and 25 mg L^{-1}, respectively. The rapid initial phosphate uptake at the beginning of the experiment for the 5 mg L^{-1} initial phosphate concentration was explained by the relatively low concentration of phosphate in the solution combined with a high level of available adsorption sites. In contrast, the extent of phosphate uptake for the 25 mg L^{-1} phosphate concentration decreased quite rapidly with time. Such adsorption behavior may be due to the high phosphate concentration relative to the number of available surface sites. The maximum phosphate uptake values were 0.06 and 0.23 mg g^{-1} for initial concentrations of 5 and 25 mg L^{-1}, respectively (Figure 4).

Effect of adsorbent dose and initial phosphate concentration on phosphate removal and phosphate uptake. Phosphate removal efficiency increased with larger shale doses (Figure 5a), and higher initial phosphate concentrations resulted in a lower percent phosphate removal at a fixed sorbent dose. The phosphate uptake interestingly displayed an opposite trend (Figure 5b) and decreased with increased shale dose, but increased with increases in initial phosphate concentration. A similar trend for all initial phosphate concentrations was clearly observed. This opposite behavior was clearly illustrated for an initial phosphate concentration of 25 mg L^{-1} (Figure 6). Phosphate uptake decreased until a shale dose of around 40 g L^{-1} was reached and then a constant value of ~0.2 mg g^{-1} was attained and, thus, indicated lower phosphate uptake efficiency at high sorbent doses. The decreased q_e values observed for shale doses between 2 g L^{-1} and 40 g L^{-1} for an initial phosphate concentration of 25 mg L^{-1} could be due to a decrease

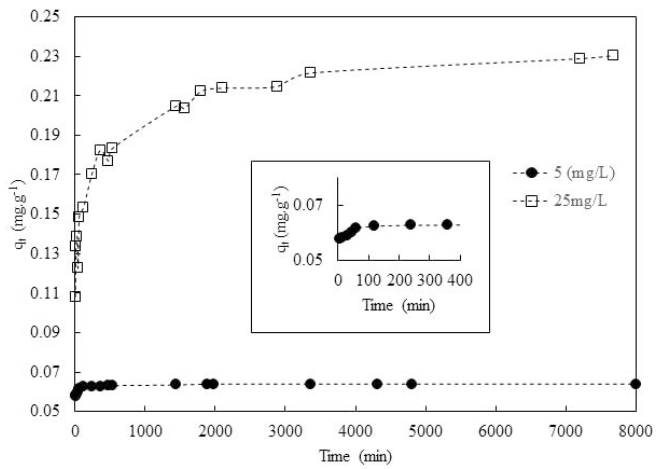

Figure 4. Effect of contact time at two initial phosphate concentrations on phosphate uptake for a shale concentration of 80 g L^{-1} at pH ≅ 7.

https://doi.org/10.1346/CCMN.2018.064118 Published online by Cambridge University Press

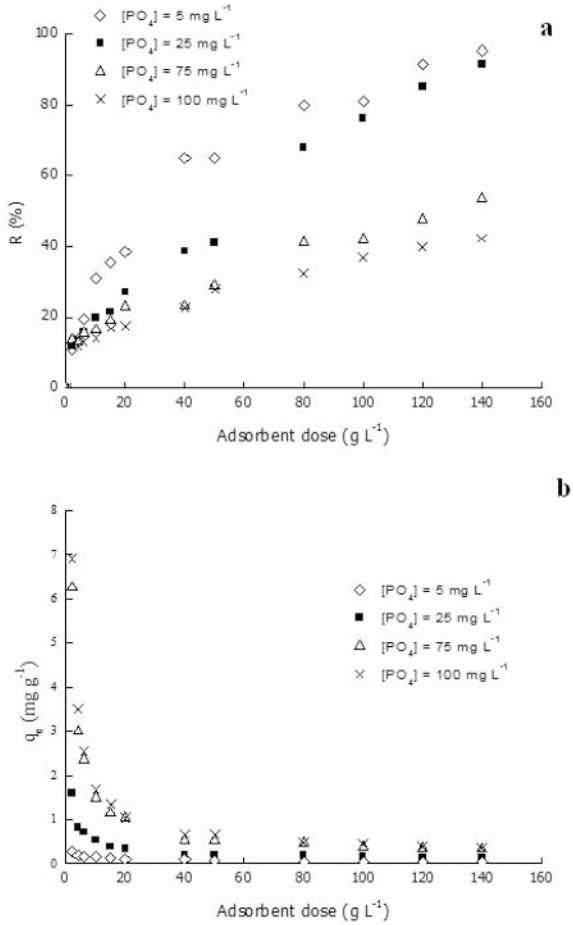

Figure 5. Effect of shale dose and initial phosphate concentration on (a) phosphate removal and (b) phosphate uptake or adsorption capacity at pH ≅ 7 and a contact time of 24 h for the shale <400 μm fraction.

in the ratio between the initial phosphate concentrations and the greater number of available shale surface sites. The maximum phosphate uptake was determined at an 80 g L^{-1} shale dose (Figure 4) and was, thus, representative of phosphate uptake values between 40 and 150 mg L^{-1}. A similar tendency was reported for phosphate adsorption to Al-based water treatment residuals (Karaca *et al*., 2006; Babatunde *et al.*, 2009; Anirudnan and Senan, 2011).

Cation concentrations as a function of pH. Dissolution of the shale was markedly pronounced at low pH values. In fact, blank experiments (*i.e*. assays performed without added phosphate) revealed high levels of total soluble Ca, Mg, and Al (Figure 7). The concentrations decreased with increased pH values and reflect a decrease in the amounts dissolved from the shale at higher pHs. A different behavior was clearly observed in the presence of phosphate. Low concentrations of dissolved Ca, Mg, Al, and Fe species were detected after reaction with phosphate at all pH values. Two hypotheses may explain these results: (i) a dissolution/precipitation phosphate removal mechanism that involves soluble Ca, Mg, Al, and Fe species released by dissolution of the shale, (ii) a surface phosphate adsorption mechanism that limits dissolution of Ca, Mg, Al, and Fe species.

Effect of pH on phosphate uptake. Experiments were carried out to investigate the effect of pH on phosphate uptake along with total soluble Ca and Al concentrations (*i.e.*, the two main species in solution after reaction with phosphate) (Figure 8). An overall decrease in phosphate uptake was observed from pH 2 to 11 followed by a strong increase in uptake at pH 12. The maximum phosphate uptake at pH 2 was ~0.26 mg g^{-1}. In addition, the Ca concentrations strongly decreased from pH 4 to 6 and then decreased to a lesser extent until pH 11. Low levels of total soluble Ca and Al species in the 6–11 pH range were probably explained by the limited solubility of these species in this pH range. Above pH 11, the dissolution of Ca and Al species explained the strong concentration increases and the concomitant increases in phosphate

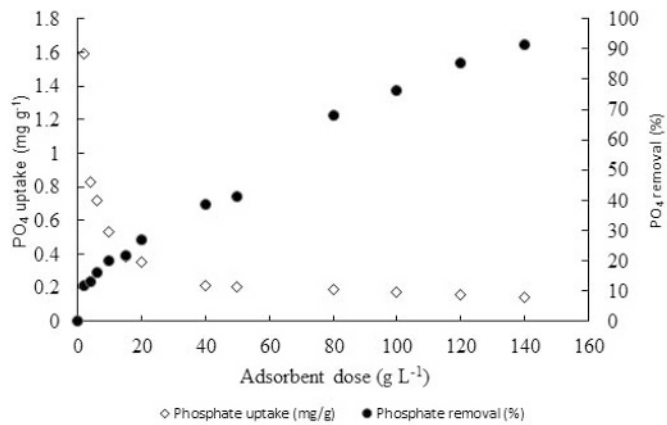

Figure 6. Effect of adsorbent dose on phosphate uptake and percent PO_4 removal for $[PO_4]_{initial}$ = 25 mg L^{-1}, a pH of ~7, and a contact time of 24 h.

https://doi.org/10.1346/CCMN.2018.064118 Published online by Cambridge University Press

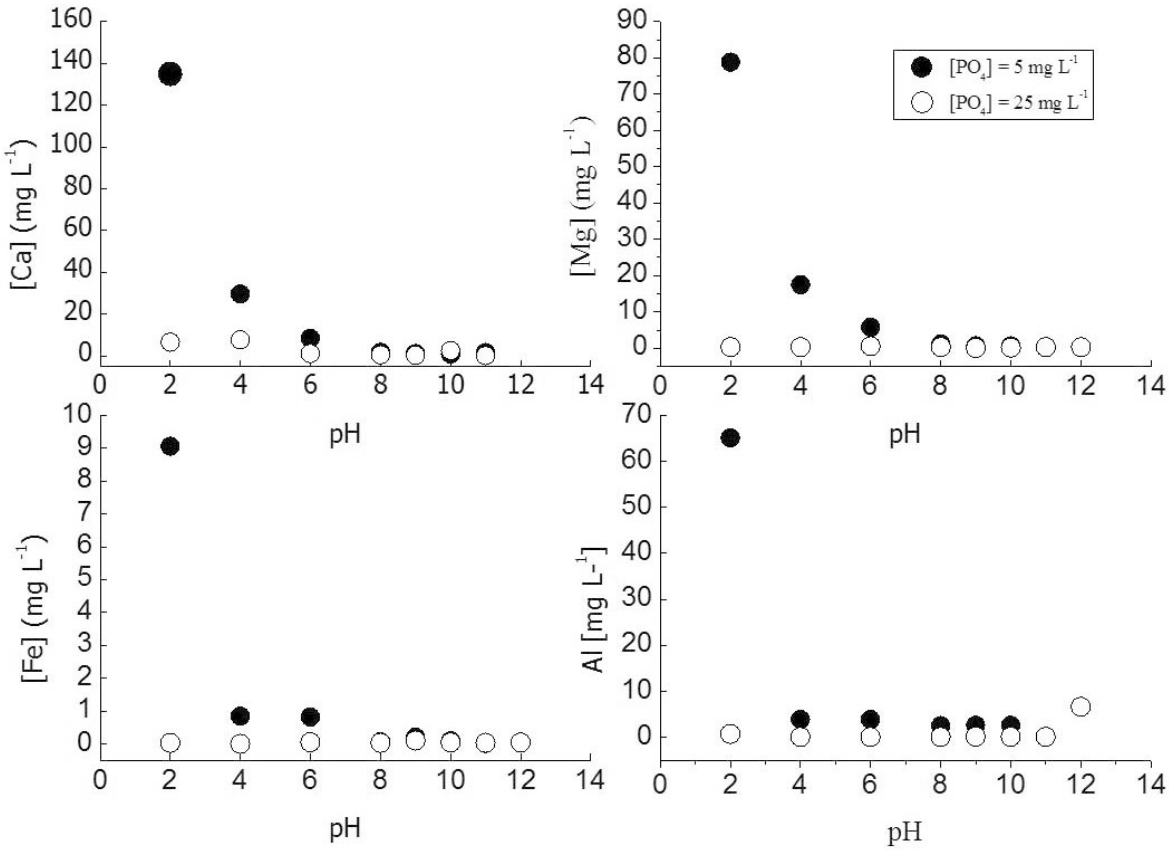

Figure 7. Concentrations of Ca, Mg, Fe, and Al in blank experiments and after reaction with a 25 mg L^{-1} initial phosphate concentration for 80 g L^{-1} of shale at pH ≅ 7, for a contact time of 24 h.

uptake. In particular, Al is well known to be dissolved under alkaline conditions and exists as the $Al(OH)_4^-$ species. Phosphate uptake as a function of pH should be carefully interpreted in view of both the complexity of the shale composition and the various processes that may be implied. In fact, both dissolution/precipitation and surface sorption processes may be involved in phosphate removal depending on the pH range. The surface charge at the solid/solution interface of minerals may also play an important role in ion adsorption. So, the overall decrease

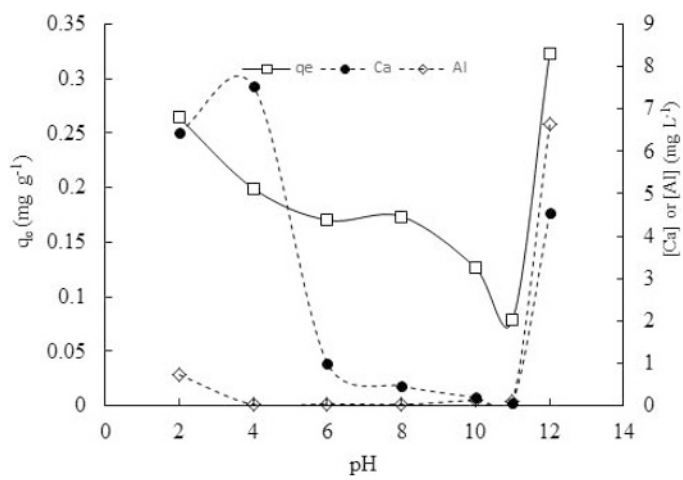

Figure 8. Phosphate uptake and aqueous Ca and Al concentrations as a function of pH after shale reaction with a 25 mg L^{-1} initial phosphate concentration for 80 g L^{-1} of shale at pH ≅ 7 for a contact time of 24 h.

https://doi.org/10.1346/CCMN.2018.064118 Published online by Cambridge University Press

Table 3. Kinetics parameters for the different models used in the present study (initial phosphate concentrations of 5 mg L^{-1} and 25 mg L^{-1}).

Model	Equation (linear form)	5 mg L^{-1}			25 mg L^{-1}		
Elovitch	$q_t = \frac{1}{b_e}\ln(t) + \frac{1}{be}\ln(a_e b_e)$	R^2 0.860	b_e 1111	A 3.2 10^{24}	R^2 0.970	b_e 60.2	a 1.93
Intra-particle diffusion	$q_t = k_i\ t^{0.5}$	R^2 0.505	C 0.124	k_i 0.003	R^2 0.805	C 0.16	k_i 0.03
Lagergren's pseudo first order	$\log(q_e - q_t) = \log q_e - \frac{k_1 t}{2.303}$	R^2 0.695	q_e 0.003	k_1 0.002	R^2 0.954	q_e 0.076	k_1 0.002
Pseudo second order	$\frac{t}{q_t} = \frac{1}{k_2 q_e^2} + \frac{t}{q_e}$	R^2 1.00	q_e 0.064	k_2 4.480	R^2 0.999	q_e 0.230	k_2 0.025

in phosphate uptake from pH 2 to 11 can be partially explained by (i) electrostatic repulsion between the negative surface sites of the various minerals in the shale and phosphate anions, which increased with increases in pH, and (ii) a decrease in positively charged sites on the goethite surface below the point of zero charge (pH_{pzc}). Most of the minerals in the shale have a pH_{pzc} value smaller than 3. This is particularly true for quartz, albite, and muscovite (Kosmulski, 2009, 2011). Only goethite has a point of zero charge value in the 7.5−9.6 pH range (Chitrakar, 2006). The decrease in phosphate uptake in the 2−10 pH range is consistent with a decrease in the number of goethite positive charge surface sites. In addition, total soluble Ca and Mg species were correlated with phosphate uptake at pH < 6 and at pH > 11, which suggests that dissolution/precipitation processes may also compete under such pH conditions (Figures 7 and 8).

Phosphate sorption kinetics. The four most common kinetics models were used to predict the adsorption kinetics of phosphate to shale, which were the Elovitch, intra-particle diffusion, Lagergren pseudo first order, and pseudo second order models (Table 3). Only the pseudo second-order model showed an excellent fit to the adsorption data ($R^2 > 0.99$) (Figure 9 and Table 3). In addition to the high R^2 correlation coefficient values obtained, the calculated q_e values agreed well with the experimental q_e values (Figure 6). The sorption rate constant k_2 value strongly decreased as initial phosphate concentrations were increased. A similar kinetics behavior has been previously reported for the adsorption of phosphate by Fe(III)/Cr(III) hydroxides (Namasivayam and Prathap, 2005), calcined Mg-Al-CO_3 layered double hydroxides (Cai *et al.*, 2012), and hydroxyaluminum and hydroxyl Fe-montmorillonite complexes (Zhu *et al.*, 2009).

Adsorption isotherms. The correlation coefficient of the Langmuir model (R^2 = 0.995) was significantly higher than the value obtained for the Freundlich model (R^2 = 0.955) (Figure 10). The q_m values from a fit of the data

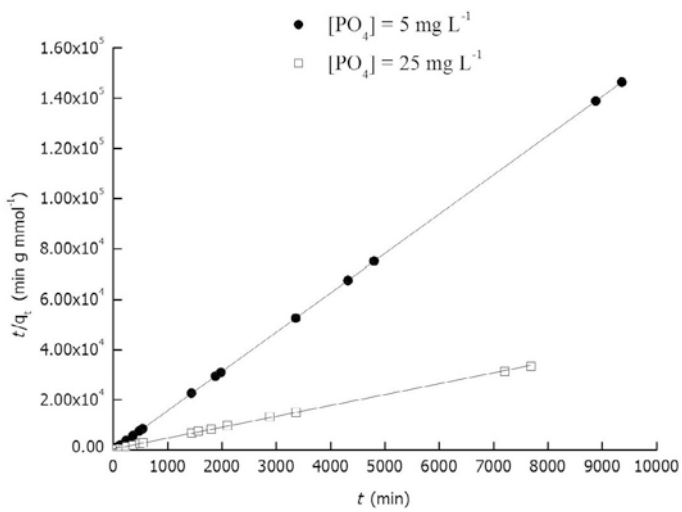

Figure 9. Kinetics modeling of phosphate sorption on shale at two initial phosphate concentrations using a pseudo-second order model for 80 g L^{-1} of shale at pH ≅ 7 for a contact time of 24 h.

https://doi.org/10.1346/CCMN.2018.064118 Published online by Cambridge University Press

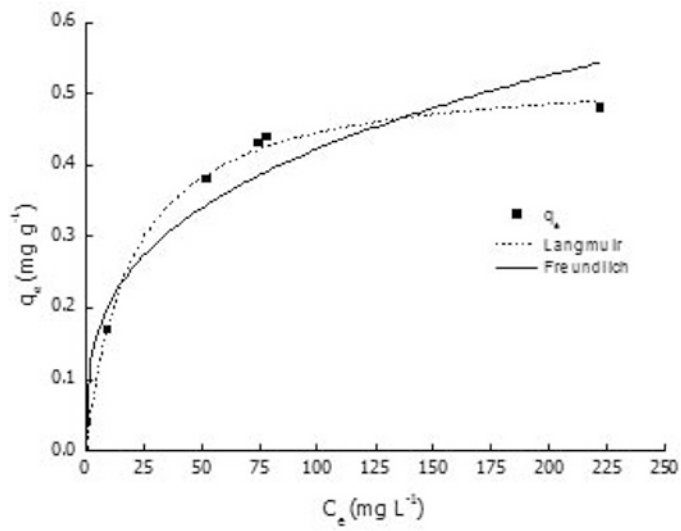

Figure 10. Phosphate adsorption isotherms for shale fitted using the Langmuir and Freundlich models for 80 g L^{-1} of shale at pH ≅ 7 for a contact time of 24 h and the <400 µm shale fraction. The fitting parameters of the Langmuir model (equation 8) were $R^2 = 0.995$, $q_{max} = 0.514$ mg g^{-1}, and $K_L = 0.061$ L g^{-1}; The parameters of the Freundlich model (equation 9) fit to the data were $R^2 = 0.955$, $n_f = 2.02$, and $K_F = 0.046$ L g^{-1}.

to the Langmuir model were ~0.51 mg g^{-1}. Increases in the initial phosphate concentration increased the maximum sorption uptake (q_{max}) by a factor of ~2. Such experimental conditions, however, did not reflect the conditions encountered in wastewaters, which have phosphate concentrations that range from 10 to 100 mg L^{-1}. Similar results were previously reported for phosphate adsorption to Fe hydroxide-eggshell waste (Chubar *et al.*, 2005), La-doped activated-C fiber (Liu *et al.*, 2011), and Fe(III)/Cr(III) hydroxide (Namasivayam and Prathap, 2005).

Phosphate adsorption under hydrodynamic conditions: Column experiments

The phosphate concentration in the column C1 outflow was determined as a function of V/V_p, where V represents the volume of solution introduced in the reactor and V_p is the pore volume of 236 mL (Figure 11). The breakthrough curve obtained during the column experiments exhibited a first plateau region, where the phosphate concentration was very low and was below the ICP-AES detection limit. This first stage was followed by an overall increase in phosphate concentrations

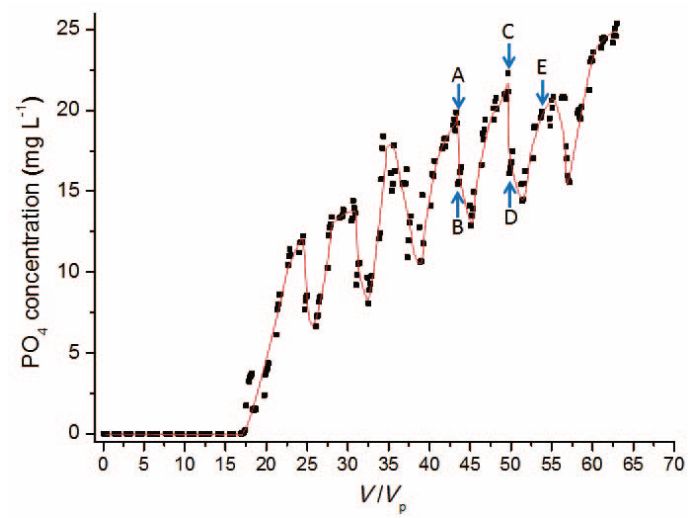

Figure 11. Evolution of phosphate concentrations in the column C1 outflow as a function of V/V_p, where V is the solution volume introduced into the column and V_p is the column pore volume. Points A, C, and E are measurements made when the phosphate flow was shut off and points B and D are measurements made after phosphate flow was restarted.

https://doi.org/10.1346/CCMN.2018.064118 Published online by Cambridge University Press

combined with a series of oscillations. Each decrease in phosphate concentration occurred exactly each time the water flow was shut off during the experiment. Each time after the water flow was restarted, the phosphate concentrations continued to decrease during a time interval that corresponded to approximately one pore volume ($V_p \cong 1$) and increased again until the next time water flow was shut off. The 104 h flow on and 64 h flow off sequences were repeated 6 times after breakthrough and corresponded to 6 oscillations (Figure 11). Finally, after 66 d of the experiment (V/Vp $\cong$ 63), the phosphate concentrations reached values very close to the 25 mg L^{-1} initial phosphate concentration (*i.e.* breakthrough) that was continuously introduced into the columns, which indicates that the shale was almost saturated with phosphate.

A V/Vp value of ~17 was measured at breakthrough and corresponded to a phosphate uptake at the breakthrough $q_{b(col1)}$ value of ~0.17 mg PO_4 g^{-1}. This value was relatively close to the phosphate uptake q_e value of ~0.2 mg g^{-1} measured in batch experiments for a shale dose greater than 40 g L^{-1} (Figure 6). The sorption capacity at breakthrough decreased with an increased flow rate. Indeed, a $q_{b(col2)}$ value of ~0.13 mg PO_4 g^{-1} was obtained for column C2, which corresponds to breakthrough at a V/Vp value of ~13 (not shown).

For V/Vp values greater than ~17, the phosphate concentrations increased rapidly and the phosphate first decrease in concentration from ~12.5 mg L^{-1} to ~7 mg L^{-1} was observed at a V/Vp value of ~24 (Figure 11). This straight decrease in phosphate concentrations was due to the increase in the HRT (equation 3) that reached 64 h when the water flow was stopped. Indeed, the contact time under static conditions was much larger than the contact time under hydrodynamic conditions (HRT $\cong$ 17 h). Most probably, the increased contact time under static conditions allowed phosphate anions to diffuse more deeply into the pores of the shale and reach adsorption sites not readily available under hydrodynamic conditions. Restarting the phosphate solution flow led rapidly to an increased phosphate concentration until the next time the peristaltic pump was shut off. The oscillation phenomenon was periodically repeated with a relatively constant amplitude that showed that the quantities of phosphate adsorbed during the 64 h static condition was almost constant. By measuring the surface area between the breakthrough curve and the horizontal segment at PO_4 = 25 mg L^{-1} for $V/V_p \in (0, 64)$, the total amount of phosphate removed of ~0.4 mg PO_4 g^{-1} was calculated (equation 5). The same value was obtained for the column experiment carried out at a 10 times higher flow rate (data not shown). This value was inside the phosphate uptake range (*i.e.*, ~0.2 mg $g^{-1} < q_e <$ ~1.6 mg g^{-1}) measured in the batch experiments (Figure 6). Drizo *et al.* (1999) performed similar column experiments using a shale collected in Scotland (Cultshill quarry, Fife). The shale was in contact with wastewater with extra phosphate of 35 and 45 mg L^{-1} added with a contact time of ~12 h. After 40 days of the Drizo *et al.* (1999) experiment, the shale was still not saturated with phosphate and both the flow rate and the phosphate concentration were doubled. The capacity of the shale to remove phosphate was estimated to be ~0.7 mg P-PO_4 g^{-1}, which is a value that is significantly higher than the value recorded in the present study (~0.13 mg P-PO_4 g^{-1}). Unfortunately, no mineralogical characterization of the shale used by Drizo *et al.* (1999) was provided. Therefore, it is rather difficult to explain why the Drizo *et al.* (1999) shale had a greater phosphate adsorption capacity than the shale used in the present study.

A more detailed analysis of the soluble Ca, Mg, P, Fe, and Al species in the column outflow was conducted using a double oscillation period between points A and E of the breakthrough curve (Figure 12). The phosphate concentrations were presented as a function of experiment time and the differences between the point A and B (or C and D) time values corresponded to the 64 h duration of the static condition after phosphate flow was shut off. Interestingly, when the flow was restarted (points B and D in Figure 12), phosphate concentrations continued to decrease for ~20 h (Figure 12, point A). The ~20 h flow duration corresponds very closely to the evacuation of one pore volume of the column. In fact, the last drop evacuated from the pore volume corresponded to water with a longer contact time with the filtration material (*i.e.*, ~84 h). This decrease in phosphate concentration was closely related to a very sharp increase in dissolved Ca and Mg (Figures 12b and 12c). The maximum Ca and Mg concentrations were at times t_1, t_2, and t_3, which exactly corresponded to the minimum phosphate concentrations. The phosphate and total dissolved Ca (or Mg) concentrations were inversely correlated in the column experiments (Figures 12b and 12c). The hypothesis now is that while the column water flow is shut off, dissolved Ca and Mg accumulate in the static mode that removed phosphate during water flow through the column. The excess dissolved Ca and Mg species that did not react with phosphate during no flow through the column would then be released when the flow was restarted. After ~1 V_p was released, the Ca and Mg concentrations decreased rapidly to more or less constant values of ~2 mg L^{-1} and 1 mg L^{-1}, respectively. These values corresponded to the solubility of the shale Ca and Mg species under hydrodynamic conditions. The total dissolved Al (Figure 12, point D) and Fe concentrations (not shown) in the column outflow were very low due to the very low solubility of Al and Fe in the 5.6 < pH < 6.6 pH range.

Relationship between mineralogy and phosphate removal

The ability of soil minerals to control phosphate adsorption was mainly studied in published articles using pure phases, such as Fe/Al (oxyhydr)oxides (Barron *et al.*, 1988; Antelo *et al.* 2005) or clay minerals

https://doi.org/10.1346/CCMN.2018.064118 Published online by Cambridge University Press

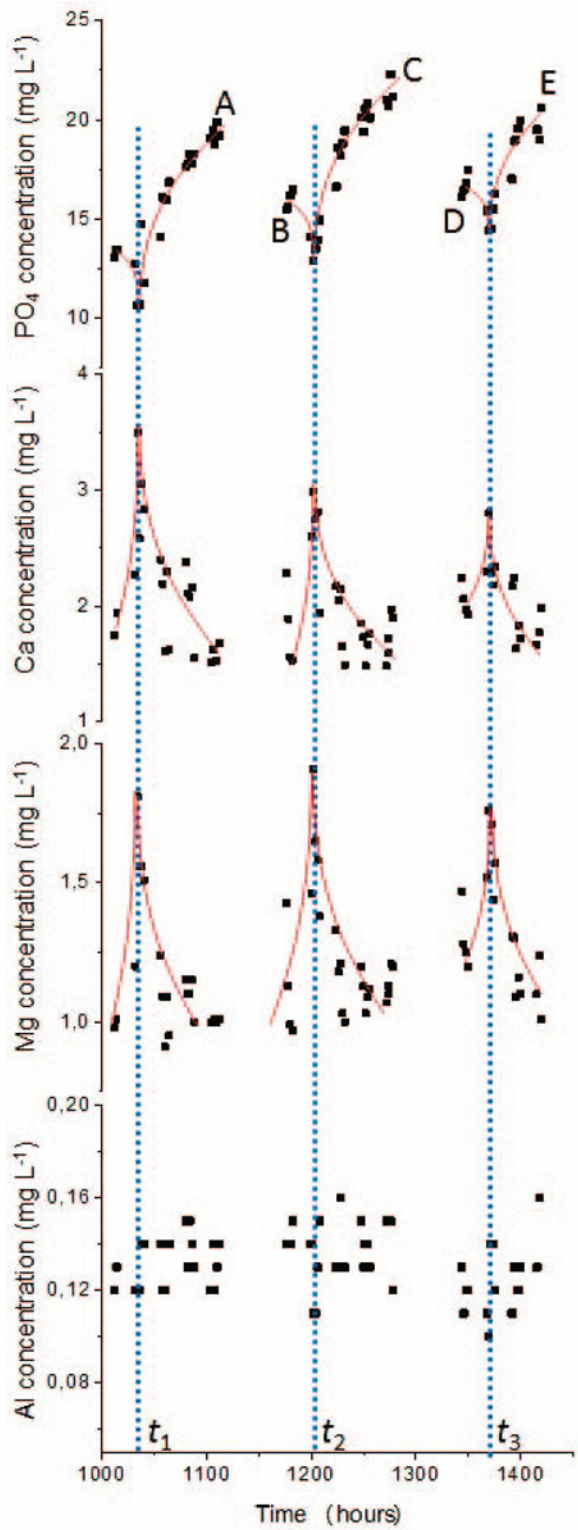

Figure 12. Evolution of the aqueous species in the column C1 outflow as a function of time. Points A, C, and E are measurements made when the phosphate flow was shut off and points B and D are measurements made after phosphate flow was restarted. Times t_1, t_2, and t_3 correspond to phosphate concentration minima.

(Baryosef *et al.*, 1988; Manning *et al.*, 1996). Shale is a complex mixture of clay minerals and Fe (oxyhydr)-oxides and both mineral types can contribute to phosphate removal. A careful examination of the results in the present study suggest that Fe (oxyhydr)oxides played a major role in phosphate removal in the 4–10 pH range. First, some studies reported that clay minerals and Fe (oxyhydr)oxides clearly differ in the dependence of phosphate uptake on pH. The phosphate adsorption capacity of clay minerals generally is markedly lower under acidic conditions, while Fe (oxyhydr)oxides, such as goethite, are characterized by progressive increases in P adsorption up to pH 3 (Huang *et al*., 2009). The phosphate adsorption capacity of shale, therefore, exhibited a pH dependence close to that reported for goethite in the pH range 4–10. Increased electrostatic repulsion between goethite and phosphate ions may explain the decreased phosphate removal by shale in the 4–10 pH range. In addition, Fe was more available in the goethite than in the structural Fe, Al, and Mg sites in clay minerals. This reinforces the hypothesis that phosphate adsorption was controlled by goethite in the 4–11 pH range. In particular, van der Zee *et al.* (2003) reported that the reactive Fe phase in a large variety of sediments was nanoparticles of goethite rather than the mixture of clay minerals in sediments. According to published data, phosphate adsorption to nanoparticles of goethite could be represented by the following equations that involve the formation of monodentate and bidentate complexes (Kubicki *et al.* 2007):

$$\equiv FeOH + H_2PO_4^- \rightleftharpoons \equiv FeOPO_2OH + H_2O \quad (9)$$

$$2 \equiv FeOH + H_2PO_4^- \rightleftharpoons \equiv (FeO)_2PO_2 + 2H_2O \quad (10)$$

The order of magnitude of PO_4 amounts removed by nanoparticles of goethite in the shale was estimated. In fact, by combining the chemical composition data reported in Table 1 with the semi-quantitative results obtained by Mössbauer spectroscopy (Table 2), the relative weight percent of goethite nanoparticles was determined to be ~3.3 %. Then, by considering a phosphate removal capacity of 33 mg g^{-1} at pH 5 (Peleka *et al.* 2009), the nanoparticles of goethite may adsorb the phosphate in a 87 mg L^{-1} phosphate solution, which is significantly greater than the phosphate concentrations used in the present study (25 mg L^{-1}). All of the goethite (αFeOOH) surface sites were probably not directly accessible in the intimate mixture of clay minerals and Fe oxides in the shale, however, which probably explains the higher phosphate adsorption capacity for a single goethite phase. Finally, the clay minerals may compete with goethite for phosphate adsorption at pHs < 4 and > 11 in batch experiments. Under such pH conditions, dissolution of both the clay minerals and the goethite occurred (Figure 7) and explains the observed greater phosphate removal (Figure 8).

https://doi.org/10.1346/CCMN.2018.064118 Published online by Cambridge University Press

CONCLUSIONS

Phosphate removal from solution by shale was studied in homogeneous batch suspensions and under static and hydrodynamic conditions in column experiments. Under both conditions, soluble species dissolved from shale and phosphate removal were clearly observed. In homogeneous suspensions at circumneutral pH, the release of dissolved Ca^{2+} and Mg^{2+} species was correlated with decreases in phosphate concentrations. In column experiments, phosphate solution and shale contact times were increased under static conditions, which favored the accumulation of dissolved Ca^{2+} and Mg^{2+} species in the reactor and consequent phosphate removal. Besides the adsorption of phosphate on shale surfaces, phosphate removal by shale dissolution followed by Ca or Mg phosphate precipitation was strongly suspected. Phosphate removal by adsorption to Fe (oxyhydr)oxides was certainly very limited in the shale examined in the present study because most of the Fe was within the structures of the clay minerals. The maximum phosphate removal by shale (q_e ~ 0.2 mg g^{-1}) was of the same order of magnitude as that measured for hydroxyapatite (Bellier and Chazarenc, 2006). Hydroxyapatite is a calcium phosphate that has already been used to successfully remove phosphates from wastewaters at the pilot scale using horizontal filters (Molle *et al.*, 2005). Because shales are readily available in many countries, the present study reinforces the assumption of Vohla *et al.* (2011) that shale and other natural minerals (Alindogan and Tumen, 2001; Jiang *et al.*, 2014; Lyngsie *et al.*, 2014**)** would be a promising material for extensive phosphate removal from water in treatments where large field surfaces and large quantities of filtration material are needed. The equivalent quantity of filtration material necessary for a population of 200 people for 4 y can be estimated using the following hypotheses (i) the experiments performed in columns can be extrapolated to a larger scale and (ii) the organic matter does not influence the phosphate removal. A quantity of ~4400 tons of shale corresponds to a surface area of ~7700 m^2 for a 50-cm thick horizontal filter (see calculation in Appendix) was determined. Extrapolation from column experiments to field experiments, however, must be performed cautiously. A short-term perspective of the present study will, thus, be to perform an experiment at an intermediate pilot scale.

APPENDIX

Calculation of the parameters for a horizontal constructed-wetland using shale.

Hypothesis 1: 2 mg P-PO_4 L^{-1} (~6 mg PO_4 L^{-1}) must be treated in the wastewater treatment plant outflow and the PO_4 adsorption capacity of the shale is 0.2 g kg^{-1} (breakthrough of the column experiments).

Hypothesis 2: One Population Equivalent (PE) will release 3 g of PO_4 per day.

The mass (m) of PO_4 (mPO_4) that has to be adsorbed to shale in 4 years is:

$mPO_4 = 3 \times 365 \times 4 = 4380$ g

and the mass of shale (m_M) needed for 200 PE combined can be calculated as follows:

$$q = \frac{mPO_4}{m_M} \times 200 \quad \Rightarrow \quad m_M = \frac{mPO_4}{q} \times 200$$

where q is the adsorption capacity at breakthrough, mPO_4 is the mass of phosphate adsorbed by the shale, and m_M is the shale mass.

Numerical application: m_M $4380/0.2 \times 200 = 4380000$ g where $m_M = 4400$ tons.

The surface area (S) used for a horizontal constructed wetland with a depth (h) of 0.5 m is:

$$S = \frac{m_M}{\rho_{app} \times h}$$

where ρ_{app} is the apparent density of the shale.

Numerical application: $S = 4400/(1.14 \times 0.5)$

$S = 7720$ m^2

ACKNOWLEDGMENTS

This work was supported by the French PIA project "Lorraine Université d'Excellence" – reference ANR-15-IDEX-04-LUE. The authors thank Ghouti Medjahdi (Centre of X-gamma Competence; UMR 7198 CNRS - Université de Lorraine, Nancy-France) for XRD analyses. The authors want to thank the staff of the technical platform "LA-ICPMS" of the GéoRessources laboratory (UMR 7359, CNRS-Université de Lorraine, France) for the chemical analyses of the shale. C. Genois from the LCPME is gratefully acknowledged for the ICP analyses. Pr C. Ruby thanks the Institute of Advanced Study of the University of Durham (UK) for a Research Fellowship during the writing of this manuscript.

REFERENCES

Ádám, K., Krogstad, T., Vråle, L., Søvik, A.K., and Jenssen, P.D. (2007) Phosphorus retention in the filter materials shell sand and filtralite P®–Batch and column experiment with synthetic P solution and secondary wastewater. *Ecology Engineering*, **29**, 200–208.

Aerts, R. and Chapin, F.S. (2000) The mineral nutrition of wild plants revisited: A re-evaluation of processes and patterns. *Advances in Ecological Research*, **30**, 2–67.

Akhurst, D.J., Jones, G.B., Clark, M., and McConchie, D. (2006) Phosphate removal from aqueous solutions using neutralized bauxite refinery residues (Bauxsol). *Environmental Chemistry*, **3**, 65–74.

Alindogan, H.S. and Tumen, F. (2001) Removal of phosphate from aqueous solutions by using bauxite, I: Effect of pH on the adsorption of various phosphates. *Journal of Chemistry Technology and Biotechnology*, **77**, 77–85.

Anirudhan, T.S. and Senan, P. (2011) Adsorption of phosphate

ions from water using a novel cellulose-based adsorbent. *Chemistry and Ecology*, **27**, 147–164.

Antelo, J., Avena, M., Fiol, S., Lopez, R., and Arce, F. (2005) Effects of pH and ionic strength on the adsorption of phosphate and arsenate at the goethite-water interface. *Journal of Colloid and Interface Science*, **285**, 476–486.

Arias, C.A. and Brix, H. (2005) Phosphorus removal in constructed Wetlands: Can Suitable alternative media be identified? *Water Science and Technology*, **51**, 267–273.

Babatunde, A.O., Zhao, Y.Q., Burke, A.M., Morris, M.A., and Hanrahan, J.P. (2009) Characterization of aluminum-based water treatment residual for potential phosphorus removal in engineered wetlands. *Environmental Pollution*, **157**, 2830–2836.

Barron, V., Herrunzo M., and Torrent, J. (1988) Phosphate adsorption by aluminous hematites of different shapes. *Soil Science Society of America Journal*, **52**, 647–651.

Baryosef, B., Kafkhafi, U., Rosenberg, R., and Sposito, G. (1988) Phosphorous adsorption by kaolinite and montmorillonite.1. Effect of time, ionic strength, and pH. *Soil Science Society of American Journal*, **52**, 1580–1585.

Bellier, N., Chazarenc, F., and Comeau, Y. (2006) Phosphorus removal from wastewater by mineral apatite. *Water Research*, **40**, 2965–2971.

Briton, G.H., Yao, B., and Ado, G. (2007) Evaluation of the Abidjan lagoon pollution. *Journal of Applied Science and Environmental Management*, **11**, 173–179.

Cai, P., Zheng, H., Wang, C., Ma, H., Hu, J., Pu, Y., and Liang, P. (2012) Competitive adsorption characteristics of fluoride and phosphate on calcinated Mg-Al-CO_3 layered double hydroxides. *Journal of Hazardous Materials*, **213–214**, 100–108.

Can, M.Y. and Yildiz, E. (2006) Phosphate removal from water by fly ash: Factorial experimental design. *Journal of Hazardous Materials*, **135**, 165–170.

Chen, S., Xu, M., Ma, Y., and Yang, J. (2007) Evaluation of different phosphate amendments on availability of metals in contaminated soil. *Ecotoxicology and Environmental Safety*, **67**, 278–285.

Chitrakar, R., Tezuka, S., Sonoda, A., Sakane, K., Ooi, K., and Hirotsu, T. (2006) Phosphate adsorption on synthetic goethite and akaganeite. *Journal of Colloid and Interface Science*, **298**, 602–608.

Chubar, N.I., Kanibolotskiy, V.A., and Strelko, V.V. (2005) Adsorption of phosphate ions on novel inorganic ions exchangers. *Colloids and Surfaces A: Physicochemical Engineering Aspects*, **255**, 55–63.

Comeau, Y., Hall, K.J., Hancock, R E.W., and Oldham, W.K. (1986) Biochemical model for enhanced biological phosphorus removal. *Water Research*, **20**, 1511–1521.

Cyrus, S.J. and Reddy, G.B. (2010) Sorption and desorption of phosphorous by shale: Batch and column experiments. *Water Science and Technology*, **61**, 599–606.

Drizo, A., Frost, C.A., Grace, J., and Smith, K.A. (1999) Physicochemical screening of phosphate-removing substrates for use in constructed wetland systems. *Water Research*, **33**, 3595–3602.

Drizo, A., Frost, C.A., Grace, J., and Smith, K.A. (2000) Phosphate and ammonium distribution in a pilot-scale constructed wetland with horizontal subsurface flow using shale as a substrate. *Water Research*, **34**, 2483–2490.

Drizo, A., Forget, C., Chapuis, R.P., and Comeau, Y. (2006) Phosphorus removal by electric arc furnace steel slag and serpentinite. *Water Research*, **40**, 1547–1554.

Huang, X., Foster, G.D., Honeychuck, R.V., and Schreifels, J.A. (2009) The maximum of phosphate adsorption at pH 4.0: Why it appears on aluminum oxides but not on iron oxides. *Langmuir*, **25**, 4450–4461.

Husein, D.Z., Al-Radadi, T., and Danish, E.Y. (2017) Adsorption of phosphate using alginate-/zirconium-grafted newspaper pellets: Fixed-bed column study and application. *Arabian Journal for Science and Engineering*, **42**, 1399–1412.

Jiang, C., Jia, L., Zhang, B., He, Y., and Kirumba, G. (2014) Comparison of quartz sand, anthracite, shale and biological ceramsite for adsorptive removal of phosphorous from aqueous solution. *Journal of Environmental Sciences*, **26**, 466–477.

Johansson, L. (1999) Blast furnace slag as phosphorus sorbents - Column studies. *Science of the Total Environment*, **229**, 89–97.

Johansson, W.L. (2006). Substrates for phosphorus removal-potential benefits for onsite wastewater treatment? *Water Research*, **40**, 23–36.

Kaasik, A., Vohla, C., Motlep, R., Mander, U., and Kirsimae, K. (2008) Hydrated calcareous oil-shale ash as potential filter media for phosphorous removal in constructed wetlands. *Water Research*, **42**, 1315–1323.

Karaca, S., Gürses, A., Ejder, M., and Açıkyıldız, M. (2006) Adsorptive removal of phosphate from aqueous solutions using raw and calcinated dolomite. *Journal of Hazardous Materials*, **128**, 273–279.

Koffi, S.O., Coffy, A.A., Villeneuve, J.P., Sess, D.E., and N'Guessan, Y.T. (2009) Pollution of a tropical lagoon by the determination of organochlorine compounds. *Tropicultura*, **27**, 77–82.

Kosmulski, M. (2009) *Surface Charging and Points of Zero Charge*, 1st ed., Surfactant Sciences Series 145, CRC Press, Boca Raton, FL.

Kosmulski, M. (2011) The pH-dependent surface charging and points of zero charge. *Journal of Colloid and Interface Science*, **353**, 1–15.

Kubicki, J.D., Kwon, K.D., Paul, K.W., and Sparks, D.L. (2007) Surface complex structures modelled with quantum chemical calculations: Carbonate, phosphate, sulphate, arsenate, and arsenite. *European Journal of Soil Science*, **58**, 932–944.

Loganathan, P., Vigneswaran, S., Kandasamy, J., and Bolan, N.S. (2014). Removal and recovery of phosphate from water using sorption. *Critical Reviews in Environmental Science and Technology*, **44**, 847–907.

Liu, J., Wan, L., Zhang, L., and Zhou, Q. (2011) Effect of pH, ionic strength, and temperature on the phosphate adsorption onto lanthanum-doped activated carbon fiber. *Journal of Colloid and Interface Science*, **364**, 490–496.

Lyngsie, G., Borggaard, O.K., and Hansen, H.C.B. (2014) A three-step test of phosphate sorption efficiency of potential agricultural drainage filter materials. *Water Research*, **51**, 256–265.

Mallet, M., Barthélémy, K., Ruby, C., Renard, A., and Naille, S. (2013) Investigation of phosphate adsorption onto ferrihydrite by X-ray photoelectron spectroscopy. *Journal of Colloid and Interface Science*, **407**, 95–101.

Manning, B.A. and Goldberg, S. (1996) Modelling arsenate competitive adsorption on kaolinite, montmorillonite, and illite. *Clays and Clay Minerals*, **44**, 609–623.

Molle, P., Liénard, A., Grasmick, A., Iwema, A., and Kabbadi, A. (2005) Apatite as an interesting seed to remove phosphorus from wastewater in constructed wetlands. *Water Science and Technology*, **51**, 193–203.

Molle, P., Martin, S., Esser, D., Besnault, S., Morlay, C., and Harouiya, N. (2011) Phosphorus removal by the use of apatite in constructed wetlands: Design recommendations. *Water Practice & Technology*, **6**, 1629–1637.

Namasivayam, C. and Prathap, K. (2005) Recycling Fe(III)/Cr(III) hydroxide, an industrial solid waste for the removal of phosphate from water. *Journal of Hazardous Materials*, **123**, 127–134.

https://doi.org/10.1346/CCMN.2018.064118 Published online by Cambridge University Press

Nedja, N. and Laskri, N. (2015) Phosphorous removal from urban wastewater *via* chemical and combined treatment against eutrophication of receiving environments. *International Journal of u- and e- Service, Science and Technology*, **8**, 303–312.

Peleka, E.N. and Deliyanni, E.A. (2009) Adsorptive removal of phosphates from aqueous solutions. *Desalination*, **245**, 357–371.

Tuo, A.D., Soro, M.B., Trokourey, A., and Bokra, Y. (2012) Assessment of waters contamination by nutrients and heavy metals in the Ebrie Lagoon (Abidjan, Ivory Coast). *Research Journal of Environmental Toxicology*, **6**, 198–209.

Tykesson, E. (2005) *Enhanced Biological Phosphorus Removal*. Doctoral Thesis, Department of Water and Environmental Engineering, Lund Institute of Technology, Lund University, Sweden.

van der Zee, C., Roberts, D.R., Rancourt, D.G., and Slomp, C.P. (2003) Nanogoethite is the dominant reactive oxyhydroxide phase in lake and marine sediments. *Geology*, **31**, 993–996.

Vohla, C.M., Kõiv, M., Bavor, H.J., Chazarenc, F., and Mander, Ü. (2011) Filter materials for phosphorus removal from wastewater in treatment wetlands-A review. *Ecological Engineering*, **37**, 70–89.

Wendling, L.A., Blomberg, P., Sarlin, T., Priha, O., and Arnold, M. (2013) Phosphorus sorption and recovery using mineral-based materials: Sorption mechanisms and potential phytoavailability, A review. *Applied Geochemistry*, **37**, 157–169.

Wood, R.B. and McAtamney, C.F. (1996) Constructed wetlands for waste water treatment: the use of laterite in the bed medium in phosphorus and heavy metal removal. *Hydrobiologia*, **340**, 323–331.

Wu, Y., Yu, Y., Zhou, J.Z., Liu, J., Chi, Y., Xu, Z.P., and Qian, G. (2012) Effective removal of pyrophosphate by Ca-Fe-LDH and its mechanism. *Chemical Engineering Journal*, **179**, 72–79.

Yao, K.M., Metongo, B.S., Trokourey, A., and Bokra, Y. (2009) Water pollution in the urban area of a tropical lagoon by oxidizable matter (Ebrie Lagoon. Ivory Coast). *International Journal of Chemical Science*, **3**, 755–770.

Zhu, M.X, Ding, K.Y., Xu, S.H., and Jiang, X. (2009) Adsorption of phosphate on hydroxyaluminum-and hydroxyiron-montmorillonite complexes. *Journal of Hazardous Materials*, **165**, 645–651.

(*Received 11 November 2017; revised 16 October 2018; Ms. 1236; AE: G. Rytwo*)